Region-specific regulation of stem cell-driven regeneration in tapeworms.

Tania Rozario[1*], Edward B. Quinn[1], Jianbin Wang[2], Richard E. Davis[2], and Phillip A. Newmark[1,3,4*]

[1]Morgridge Institute for Research, Madison, WI, USA, [2]Department of Biochemistry and Molecular Genetics, RNA Bioscience Initiative, University of Colorado School of Medicine, Aurora, CO, USA, [3] Howard Hughes Medical Institute, [4]Department of Integrative Biology, University of Wisconsin-Madison, Madison, WI, USA.

* corresponding authors

Email: pnewmark@morgridge.org

trozario@morgridge.org

Abstract

Tapeworms grow at rates rivaling the fastest-growing metazoan tissues. To propagate they shed large parts of their body; to replace these lost tissues they regenerate proglottids (segments) as part of normal homeostasis. Their remarkable growth and regeneration are fueled by adult somatic stem cells, that have yet to be characterized molecularly. Using the rat intestinal tapeworm, *Hymenolepis diminuta*, we find that regenerative potential is regionally limited to the neck, where head-dependent extrinsic signals create a permissive microenvironment for stem cell-driven regeneration. Using transcriptomic analyses and RNA interference, we characterize and functionally validate regulators of tapeworm growth and regeneration. We find no evidence that stem cells are restricted to the regeneration-competent neck. Instead, lethally irradiated tapeworms can be rescued when cells from either regeneration-competent or regeneration-incompetent regions are transplanted into the neck. Together, the head and neck tissues provide extrinsic cues that regulate stem cells, enabling region-specific regeneration in this parasite.

Introduction

Tapeworms are parasitic flatworms that infect humans and livestock, causing lost economic output, disease, and in rare cases, death[1]. These parasites are well known for their ability to reach enormous lengths. For example, humans infected with the broad or fish tapeworm, *Diphyllobothrium latum*, harbor parasites that average 6 m in length[2]. It is less commonly appreciated that tapeworms can regenerate to accommodate their multi-host life cycle. Adult tapeworms in their host intestines develop proglottids (segments) that are gravid with embryos. Tapeworms pinch off the posterior and gravid sections of their body, which exit with the host excrement, to be eaten by a suitable intermediate host that supports larval tapeworm development. Despite losing large body sections, the tapeworm does not progressively shorten; instead, it regenerates proglottids, allowing the worms to maintain an equilibrium length. Despite this remarkable biology, tapeworms are an unexplored animal model in the study of regenerative behaviors.

Up to the 1980s the rat intestinal tapeworm, *Hymenolepis diminuta*, had been a favorite model organism among parasitologists. *H. diminuta* grows rapidly–within the first 15 days of infection, it produces up to 2200 proglottids, increases in length by up to 3400 times, and weight by up to 1.8 million times [3]–and is easily propagated in the laboratory. Foundational work on their biochemistry, ultrastructure, and developmental biology enriched our understanding of these tapeworms[4]. However, with the dawn of the molecular age and the rise of genetic model organisms, *H. diminuta* was essentially left behind. Here, we show that *H. diminuta* is an excellent, tractable model for the study of stem cells and regeneration, with the power to inform us about parasite physiology.

50 As an obligate endoparasite, adult *H. diminuta* will expire once its host rat dies. However,
51 the lifespan of *H. diminuta* can be greatly increased via regeneration. A single adult tapeworm can
52 be serially amputated and transplanted into a new host intestine, where the fragment can regenerate
53 into a mature tapeworm even after 13 rounds of amputation over 14 years[5]. These observations
54 have led to speculation that *H. diminuta* may be inherently immortal. This situation is reminiscent
55 of the free-living cousins of tapeworms: freshwater planarians like *Schmidtea mediterranea*, which
56 reproduce indefinitely by fission, and can regenerate their whole body from tiny fragments.

57 Planarian immortality and regeneration are enabled by adult somatic stem cells called
58 neoblasts[6-8]. These stem cells are the only dividing undifferentiated cells within the soma. Like
59 planarians, *H. diminuta* maintains a population of neoblast-like adult somatic stem cells[3] that are
60 likely responsible for their growth and regenerative ability. Recently, stem cells of multiple species
61 of parasitic flatworms have been described[9-13]. Stem cells play crucial roles in parasite
62 development, transmission, homeostasis, and even disease. For example, stem cells enable prolific
63 reproduction and longevity[14], mediate host-parasite interactions[15], and allow metastatic parasite
64 transmission in host tissues[16]. How stem cells may regulate regeneration in parasites such as
65 tapeworms is largely unexplored and the subject of this study.

66 We use *H. diminuta,* to investigate the molecular basis of tapeworm regeneration. We
67 have established and refined experimental tools such as transcriptomics, *in vitro* parasite culture,
68 whole-mount and fluorescent RNA *in situ* hybridization (WISH and FISH), cycling-cell tracing
69 with thymidine analogs, RNA interference (RNAi), and cell transplantation, all described in this
70 work. We determine that the ability to regenerate is regionally limited to the neck of adult *H.*
71 *diminuta*. However, regeneration from the neck is finite without signals from the tapeworm head.
72 Using RNA sequencing (RNA-seq), we identify and characterize various markers of the somatic

73 cycling-cell population, which includes tapeworm stem cells. Using RNAi, we functionally
74 validate molecular regulators of growth and regeneration. However, our analyses failed to
75 uncover a neck-specific stem cell population that explains the regional regenerative ability
76 displayed by *H. diminuta.* Instead, we show that cells from both regeneration-competent and
77 regeneration-incompetent regions of *H. diminuta* have stem cell ability and can restore viability
78 to lethally irradiated tapeworms. Our results show that extrinsic signals present in the tapeworm
79 neck, rather than specialized stem cells, confer region-specific regenerative ability in this
80 tapeworm.

81 **Results**

82 The anatomy of adult *H. diminuta* consists of a head with four suckers, an unsegmented
83 neck, and a body with thousands of proglottids/segments that grow and mature in an anterior-to-
84 posterior direction[3,17] (Fig. 1a). What regions of the tapeworm body are competent to regenerate?
85 In order to test regeneration competency, it is necessary to grow tapeworms *in vitro* instead of in
86 the intestine, where the suckers are required to maintain parasites *in vivo*. We established *H.*
87 *diminuta in vitro* culture conditions modified from Schiller's method[18] and tested the regeneration
88 competence of 1 cm amputated fragments (Fig. 1b-c). The anterior-most fragments
89 (head+neck+body) were competent to regenerate, confirming *in vivo* observations using
90 amputation and transplantation[5,19]. Anterior fragments that were first decapitated (neck+body)
91 were also competent to regenerate. In contrast, "body only" fragments failed to regenerate
92 proglottids. All amputated fragments could grow in length (Fig. 1d), differentiate mature
93 reproductive structures, and mate. However, the neck is necessary for regeneration of new
94 proglottids over time. In no case did we observe head regeneration. Furthermore, amputated heads
95 alone could not regenerate *in vitro* (data not shown) nor *in vivo*[5]. The neck is also sufficient for
96 proglottid regeneration as 2 mm "neck only" fragments regenerated an average of 383 proglottids
97 (SD=138, N=4, n=20) after 12 days *in vitro* (Fig. 1e).

98 Previous *in vivo* studies have shown that *H. diminuta* can regenerate after serial rounds of
99 amputation and transplantation for over a decade[5] and perhaps indefinitely. Using *in vitro* culture,
100 we confirmed that anterior fragments of *H. diminuta* can regenerate after at least four rounds of
101 serial amputation (Fig. 1f-g). Decapitated (-head) fragments regenerated proglottids after the first
102 amputation; however, re-amputation abrogated regeneration (Fig. 1f-g). After decapitation, a
103 definitive neck could not be maintained and eventually, the whole tissue was comprised of

104 proglottids (Fig. 1–figure supplement 1). Without the head, proglottid regeneration from the neck
105 is finite. Thus, while the neck is both necessary and sufficient for proglottid regeneration, the head
106 is required to maintain an unsegmented neck and for persistent regeneration.

107 If signals from the head regulate regeneration, is regenerative potential asymmetric across
108 the anterior-posterior (A-P) axis of the neck? We subdivided the neck into three 1 mm fragments
109 and found that the most-anterior neck fragments regenerated more proglottids than the middle or
110 posterior neck fragments (Fig. 1h-i). Thus, regeneration potential is asymmetric across the neck
111 A-P axis with a strong anterior bias.

112 Since the neck is the only region competent to regenerate, are stem cells preferentially
113 confined to the neck? In lieu of specific molecular markers for stem cells, we examined the
114 distribution of all cycling cells in adult tapeworms. In *H. diminuta,* the only proliferative somatic
115 cells are undifferentiated[20,21], thus, cycling somatic cells include tapeworm stem cells and any
116 dividing progeny. To label cycling cells, we used two methods: uptake of the thymidine analog F-
117 *ara*-EdU[22] to mark cells in S-phase and FISH against cell cycle-regulated transcripts, such as the
118 replication licensing factor *minichromosome maintenance complex component 2* (*mcm2*) and
119 *histone h2b* (*h2b*), which are conserved stem cell markers in free-living and parasitic flatworms[9,23].
120 We detected cycling somatic cells throughout the tapeworm body (Fig. 2a-b). Contrary to previous
121 results[20], we also detected cycling cells in the head, though in small numbers (Fig. 2a). The scarcity
122 of these cells may be the reason they were originally missed. Taken together, cycling cells are
123 present in all regions, regardless of regeneration competence.

124 To further our understanding of how tapeworm stem cells are distributed and regulated, we
125 sought to identify stem cell markers. Stem cell genes have been discovered previously in flatworms
126 by identifying transcripts downregulated after exposure to irradiation, which depletes cycling

127 cells[9,23,24]. Exposing *H. diminuta* to 200 Gy X-irradiation reduced the number of cycling cells by
128 91±6% after 3 days (Fig. 2c-d) and caused stunted growth and regeneration (Fig. 2–figure
129 supplement 1). We leveraged the sensitivity of *H. diminuta* to irradiation in order to identify new
130 molecular markers of cycling somatic cells by RNA-seq (Fig. 2e). A *de novo* transcriptome of
131 14,346 transcripts was assembled (see Materials and Methods) to which sequencing reads were
132 mapped. We identified 683 transcripts that were irradiation sensitive (downregulated; FDR ≤0.05)
133 (Supplemental Table 1). Expression of irradiation-sensitive genes by WISH was indeed reduced
134 after exposure to irradiation, validating our RNA-seq approach (Fig. 2–figure supplement 2).

135 Two rounds of expression screening were then applied to hone in on cycling-cell genes
136 from our irradiation-sensitive dataset (Fig. 2e). The position of cycling cells in the neck is spatially
137 restricted in a conserved pattern[25] (Fig. 3a): cycling cells reside in the neck parenchyma bounded
138 by the nerve cords and are absent from the animal edge where muscle and tegument (parasite skin)
139 are located[20]. Among 194 irradiation-sensitive transcripts that displayed clear WISH patterns, 63%
140 were expressed in the neck parenchyma, though in a variety of patterns (Fig. 3–figure supplement
141 1). 13% showed similar patterns to *h2b* and *mcm2* (Fig. 3b-c, Fig. 3–figure supplement 1b). These
142 include the nucleic acid binding factor *Zn finger MYM type 3* (*zmym3)*, the transcription factor
143 *suppressor of hairy wing* (*su(Hw)*)*, NAB co-repressor domain 2 superfamily member* (*nab2*), and
144 nuclear lamina component *laminB receptor* (*lbr*). 25% of irradiation-sensitive genes, were
145 expressed in a minority of cells in the neck parenchyma (Fig. 3–figure supplement 1c). 24% were
146 expressed within the parenchyma and more broadly toward the animal edge (Fig. 3–figure
147 supplement 1d). The remainder represented genes expressed at segment boundaries or in
148 differentiated tissues (Fig. 3–figure supplement 1e-f). In conclusion, irradiation-sensitive

149 transcripts identified by RNA-seq likely represent markers for stem cells, progenitors, and even
150 differentiated cells that were lost or compromised following irradiation.

151 To focus on genes with enriched expression in cycling cells, we performed double FISH
152 (dFISH) with candidate genes and either *h2b* or *mcm2,* which we used interchangeably as they are
153 co-expressed in the neck parenchyma (Fig. 3–figure supplement 2). After dFISH for 53 candidates,
154 72% of genes tested were co-expressed in cycling cells (Fig. 3–figure supplement 3a,
155 Supplemental Table 2). The irradiation-sensitive transcripts from Fig. 3c were indeed colocalized
156 in cycling somatic cells (Fig. 3d). One gene, the homeobox factor *prospero* (*prox1*), was expressed
157 exclusively in a subset of cycling cells (Fig. 3–figure supplement 3b). We confirmed that genes
158 whose expression only partially overlapped in the neck parenchyma, such as the Zn finger-
159 containing gene *HDt_10981* and *palmitoyl-protein thioesterase 1 (ppt1)*, were expressed in both
160 cycling cells and non-cycling cells (Fig. 3–figure supplement 3c). We propose that these genes
161 likely represent lineage-committed stem cells or progenitors for tissues such as muscle, neurons,
162 tegument, or protonephridia. 28% of irradiation-sensitive genes were predominantly expressed in
163 non-cycling cells that were juxtaposed to cycling cells (Fig. 3–figure supplement 3d). In summary,
164 our analysis revealed a heterogeneous and complex mixture of cell types or states in the neck
165 parenchyma as well as within the cycling-cell population.

166 What role(s) do the newly identified cycling-cell genes play during regeneration? We
167 developed an RNAi protocol to knock down target genes, confirm knockdown by quantitative PCR
168 (Fig. 4–figure supplement 1), and assay for defects in growth and regeneration (Fig. 4a). As a proof
169 of principle, we knocked down *h2b,* which should compromise growth due to cycling-cell loss, as
170 observed in other flatworms[15,23]. Knockdown of *h2b, zmym3,* and *su(Hw)* each resulted in
171 diminished growth and regeneration (Fig. 4b-c). The number of proglottids regenerated was also

172 reduced, but could not be quantified as many RNAi worms were so thin and frail that proglottid
173 definition was lost.

174 Are these RNAi-induced failures in growth and regeneration due to defects in the cycling-
175 cell population? RNAi knockdown of *h2b, zmym3,* and *su(Hw)* severely reduced the number of
176 cycling cells in the neck (Fig. 4d-e). The loss of F-*ara*-EdU uptake after RNAi could be due to a
177 failure of proliferation or to loss of the cell population. Thus, we performed WISH to detect the
178 cycling-cell marker *mcm2* and observed a reduction of this cell population after RNAi (Fig. 4f).
179 Taken together, *h2b, zmym3,* and *su(Hw)* are necessary for the maintenance of the cycling-cell
180 population, including stem cells, in *H. diminuta*.

181 Although we have identified heterogeneity within the cycling-cell population of the neck
182 parenchyma and uncovered genes that are required for growth and regeneration, it remains unclear
183 why regeneration competence is restricted to the neck. By WISH all cycling-cell genes, including
184 *zmym3* and *su(Hw)*, were detected throughout the whole tapeworm body (Fig. 4g). Since we
185 observed an anterior bias in regenerative ability (Fig. 1h-i), we hypothesized that RNA-seq may
186 reveal an anteriorly biased stem cell distribution. Thus, we performed RNA-seq of 1 mm anterior,
187 middle, and posterior neck fragments (Fig. 1h), and identified 461 anterior-enriched and 241
188 anterior-depleted transcripts (Supplemental Table 3). By WISH, anterior-enriched and anterior-
189 depleted transcripts were often detected in corresponding gradients (Fig. 5a), but in patterns that
190 were excluded from the neck parenchyma. When we overlaid the anterior-enriched and -depleted
191 datasets with our irradiation-sensitive dataset, the majority of anterior-enriched transcripts (88%)
192 were not irradiation sensitive (Fig. 5b). Our results suggest that the A-P polarized signals across
193 the neck region arise predominantly within the non-cycling compartments.

194 Since our RNA-seq analysis identified 57 transcripts that were anterior enriched and
195 irradiation sensitive, we examined expression patterns within this category. We found 15 genes
196 expressed in a subset of cells within the neck parenchyma (Fig. 5c), but 7/8 genes tested were not
197 expressed in cycling cells (Fig. 5d, Supplemental Table 2). Only one gene, *prox1,* was co-
198 expressed in cycling cells (Fig. 3–figure supplement 3b). These analyses have not revealed an
199 anteriorly biased subpopulation of stem cells that confer regenerative ability.

200 With no evidence for a unique neck-specific subpopulation of stem cells, we hypothesized
201 that stem cells may be distributed throughout the tapeworm, but that extrinsic signals functioning
202 in the neck are necessary to instruct stem cell behavior and/or proglottid regeneration. We designed
203 a functional assay to test populations of cells for the ability to rescue regeneration, modelled after
204 similar experiments performed on planarians[8]. We exposed tapeworms to a lethal dose of
205 irradiation, injected cells from wild-type donors into the neck region, amputated 5 mm anterior
206 fragments, and assayed rescue of lethality and regeneration after 30 days *in vitro*. Remarkably,
207 bulk-cell transplants were able to either partially or fully rescue irradiated worms that were
208 destined to die (Fig. 6a, c). "Full" rescue was ascribed to worms with normal adult appearance
209 whereas "partial" rescue was assigned to cases in which proglottids were regenerated but the
210 worms displayed abnormalities, like contracted necks (Fig. 6–figure supplement 1a). We did not
211 observe any proglottid regeneration in irradiated worms with or without buffer injection (Fig. 6a,
212 c).

213 Is the rescue ability described above dependent on tapeworm cycling cells? We exposed
214 donors to F-*ara*-EdU for 1 hr, to label cycling cells prior to transplantation into irradiated hosts
215 (Fig. 6–figure supplement 1b). Though bulk-cell transplants were performed, injection sites
216 contained 0, 1, or small groups of F-ara-EdU^{+} cells immediately after transplantations (Fig. 6–

217 figure supplement 1c), likely due to technical challenges. Despite this issue, we were able to detect
218 large colonies of F-ara-EdU^{+} cells 3 days post-transplantation (Fig. 6–figure supplement 1d). We
219 also observed that some labeled cells were incorporated into terminally differentiated tissues at the
220 animal edge (Fig. 6–figure supplement 1d: inset). Thus, cycling cells from donors are able to
221 become established and differentiate inside the irradiated host.

222 To test if the cycling-cell population is necessary to rescue lethally irradiated tapeworms,
223 we depleted cycling cells from donor worms using hydroxyurea (HU), which resulted in 96±3%
224 loss of cycling cells after 6 days (Fig. 6–figure supplement 1e-f). Cycling cells are essential for
225 rescue of regeneration as injected cells from HU-treated donors rescued only 1% of the time,
226 compared to 24% rescue using cells sourced from sister donors that did not receive the drug (Fig.
227 6b-c). HU was used to deplete cycling cells instead of irradiation in order to avoid inducing DNA
228 damage in the transplanted cells. Cells transplanted from HU-treated donors had otherwise
229 comparable morphology to untreated cells (Fig. 6–figure supplement 1g). Our results suggest that
230 tapeworm cycling cells contain *bona fide* stem cell activity.

231 With this functional assay in hand, we examined the rescue ability of cells from anterior
232 donor tissues (including the regeneration-competent neck) compared to posterior donor tissues
233 (which are regeneration incompetent). Cells from either region were able to rescue regeneration in
234 lethally irradiated tapeworms (Fig. 6b-c). These results support the idea that the regeneration
235 competence of the neck is due to extrinsic signals that regulate regeneration, rather than intrinsic
236 properties of stem cells in the neck region. It appears that in tapeworms, location matters
237 enormously: the head and neck environment provide cues that regulate the ability of stem cells to
238 regenerate proglottids, even though cycling cells (and likely stem cells), are not anatomically
239 confined.

240 **Discussion**

241 Across the flatworm phylum, both free-living and parasitic worms maintain stem cells
242 throughout adulthood but display a range of regenerative abilities. The freshwater planarian *S.*
243 *mediterranea* can regenerate its whole body from tiny amputated fragments. The blood fluke
244 *Schistosoma mansoni* cannot regenerate after amputation, though it does employ adult somatic
245 stem cells in other ways, such as to repair injury[26] and produce prodigious numbers of eggs[27]. Prior
246 to this study, the regenerative ability of tapeworms had never been comprehensively tested.
247 Although it was known that anterior fragments containing the head, neck, and immature proglottids
248 could regenerate into fully mature tapeworms once transplanted into a rat intestine[5,19], fragments
249 lacking heads could not be tested for regenerative ability using transplantation. Attempts were
250 made to suture *H. diminuta* fragments with mutilated or removed heads into a rat intestine but
251 these fragments were invariably flushed out[19]. Here we employ a robust *in vitro* culture system
252 that allowed us to test regeneration of any amputated *H. diminuta* fragment for the first time. We
253 show that the neck is both necessary and sufficient for proglottid regeneration, though this
254 regenerative ability is ultimately finite without regulatory signals that depend on the presence of
255 the head. *H. diminuta* is an intriguing model to discover signals that both drive and limit
256 regenerative ability.

257 During homeostasis, the neck of *H. diminuta* serves as a "growth zone" from which
258 proglottids are thought to bud one at a time[28], thus, it makes intuitive sense that this tissue would
259 retain the ability to regenerate proglottids post-amputation. Furthermore, cells with the typical
260 morphology of stem cells are resident in the neck[20]. However, we find that cycling cells are present
261 in all regions regardless of regenerative competence. Thus, it was necessary to embark on a more

262 thorough characterization of tapeworm cycling cells to understand how *H. diminuta* may regulate
263 stem cells and enable proglottid regeneration.

264 Adult somatic stem cells in free-living flatworms have already been well described
265 molecularly, and share many conserved regulators. However, parasitic flatworms have lost some
266 stem cell genes (e.g. *piwi*, *vasa*, and *tudor*)[29] but retained others (e.g. *argonaute*, *fgfr*)[9,10]. In larvae
267 of the tapeworm *Echinococcus multilocularis*, many putative stem cell markers show limited
268 overlapping gene expression patterns, pointing to a heterogenous cycling-cell population[10]. We
269 depleted cycling cells in *H. diminuta* using irradiation and employed RNA-seq to uncover potential
270 stem cell regulators in an unbiased fashion. Though irradiation may have secondary effects beyond
271 stem cell depletion[23], this approach allowed us to generate an initial list of candidate tapeworm
272 stem cell genes. Similar to other flatworms[23,30-32], we find that the cycling somatic cell population
273 is heterogenous, though we also identified 23 genes, including *zmym3* and *su(Hw)*, that label all
274 cycling cells in adult *H. diminuta*.

275 Importantly, we were able to use RNAi to functionally verify that cycling cell genes like
276 *zmym3* and *su(Hw)* are critical for stem cell maintenance and that inhibition of these genes leads
277 to impaired growth and regeneration. In other systems, *zmym3* has been shown to regulate cell
278 cycle progression[33] and DNA repair[34], whereas *su(Hw)* binds to *gypsy* insulator sequences to
279 regulate chromatin silencing[35]. Similar functions for these genes may be conserved in *H. diminuta*
280 as cell cycle regulation, DNA repair, and chromatin silencing are likely important for the regulation
281 of tapeworm stem cells. RNAi has been demonstrated previously in other tapeworm species[36-38],
282 though not in *H. diminuta.* RNAi has not been widely adopted for studying tapeworm biology due
283 to technical challenges like poor knockdown efficacy, inefficient penetrance, and the difficulty of
284 *in vitro* culture. Taking advantage of the robust *in vitro* culture of *H. diminuta*, our RNAi scheme

285 can be expanded to ascertain functions for many parasitic flatworm genes that thus far have been
286 refractory to functional analyses.

287 Our screening strategy allowed us to verify 38 genes with enriched expression in some or
288 all cycling cells; however, none of these genes were expressed exclusively in the neck. Since we
289 had observed that regenerative ability was anteriorly biased across the neck, we attempted to
290 leverage this observation and query whether a subpopulation of pluripotent cycling cells may be
291 asymmetrically distributed across the neck and would be identifiable by RNA-seq. Through A-P
292 transcriptional profiling of the neck, we identified 461 anterior-enriched genes but the vast
293 majority of them were neither irradiation-sensitive nor detected in cycling cells by dFISH. Thus,
294 a subpopulation of neck-resident pluripotent stem cells, seems unlikely to explain the region-
295 specific regenerative ability of tapeworms. Nonetheless, our study does not exclude the existence
296 of a subpopulation of pluripotent stem cells that may be stably maintained in the adult. Future
297 studies using single-cell RNA sequencing are likely to provide a thorough characterization of adult
298 somatic stem cells in *H. diminuta*, as has been the case for planarians[31,32,39].

299 Is the neck competent to regenerate because of a unique stem cell population that has yet
300 to be identified, or because of signals extrinsic to stem cells that make the neck permissive for
301 regeneration? Tapeworms exposed to a lethal dose of irradiation prior to amputation are not
302 competent to regenerate and will eventually degenerate and die. However, transplantation of cells
303 from wild-type donors into the necks of irradiated tapeworms rescued lethality and regeneration.
304 This rescue ability is severely compromised if donor worms are first depleted of cycling cells using
305 drug treatment with HU, suggesting that some or all cycling cells have stem cell ability.
306 Interestingly, stem cell ability is not restricted to cells from regeneration-competent regions: cells
307 from posterior tissues that do not regenerate proglottids are still able to rescue regeneration when

308 transplanted into the neck. These data strongly suggest that the microenvironment within the neck
309 confers regenerative ability to this region.

310 The interplay between intrinsic and extrinsic stem cell regulatory signals has been shown
311 to play important roles in regeneration. Head regeneration was induced in three naturally
312 regeneration-deficient planarian species by manipulating the gradient of Wnt signaling by RNAi[40-
313 42]. These planarians maintain pluripotent stem cells but do not normally regenerate heads from
314 posterior tissues due to inappropriately high levels of Wnt signaling, which inhibit anterior
315 regeneration. As in planarians, gradients of Wnt signaling delineate A-P polarity in tapeworms[43].
316 Our transcriptional profiling of the neck A-P axis has already revealed hundreds of candidate genes
317 with polarized expression profiles. Future experiments will help clarify how Wnt signaling and
318 other A-P axis regulation in the neck impacts tapeworm regeneration.

319 Several plausible models can explain region-specific regeneration in *H. diminuta*. Head-
320 dependent signals may create gradients across the neck that inhibit proglottidization and are
321 necessary to maintain the neck as an unsegmented tissue. Proglottids can only form once the
322 inhibitory signals are sufficiently diminished (Fig. 6d). In this model, the neck is competent to
323 regenerate because of its juxtaposition to the head. After decapitation, the head-dependent signals
324 eventually dissipate and segmentation signals dominate at the expense of the neck. The cellular
325 source of the head-dependent signals and their molecular identity will be exciting avenues for
326 future research.

327 In addition to its function in maintaining the neck, the head may also play a role in stem
328 cell regulation (Fig. 6e). The head may regulate a niche (directly or indirectly) that is necessary
329 for the maintenance of pluripotency in the neck. In this model, stem cells are collectively
330 pluripotent only when they receive head-dependent niche signals, thus limiting regenerative

331 potential to the neck. Alternatively, stem cells may depend on a local niche that is independent of
332 the head. In this model, stem cells have the capacity to form all cell lineages from any amputated
333 fragment; however, the extrinsic signals that activate proglottid formation are restricted to the
334 posterior neck region. Identifying the stem cell niche and its relationship to the head and neck
335 microenvironment will provide crucial insights into our understanding of tapeworm regeneration.
336

337 **Conclusion**

338 Our study shows that *H. diminuta* is a powerful developmental model for understanding
339 intrinsic and extrinsic regulation of stem cells and regeneration. The regionally limited
340 regenerative biology of *H. diminuta* and the technical advances put forth in this work show that
341 we can exploit this tapeworm to understand the complexities of stem cell regulation in parasites.
342 We defined heterogenous stem cells that are collectively pluripotent but that require extrinsic head-
343 dependent signals to enable persistent proglottid regeneration. Understanding how the stem cell
344 niche we describe is regulated may have broad implications for elucidating stem cell biology in
345 parasitic flatworms, as well as other regenerative animals.
346

347 **Acknowledgements**

348 We thank: members of the Newmark lab, especially Melanie Issigonis and Umair Khan,
349 for discussions and comments on the manuscript; Alvaro Hernandez (Roy J. Carver Biotechnology
350 Center, University of Illinois at Urbana-Champaign) for RNA-seq; and Bret Duffin (Morgridge
351 Institute for Research) for invaluable assistance with irradiation. This work was supported by NIH
352 R21AI119960. PAN is an investigator of the Howard Hughes Medical Institute.
353

354 **Materials and Methods**

355 Animal care and use

356 Infective *H. diminuta* cysts were obtained from Carolina Biological (132232). To obtain
357 adult tapeworms, 100-400 cysts were fed to Sprague-Dawley rats by oral gavage in ~0.5 mL of
358 0.85% NaCl. Rats were euthanized in a CO_2 chamber 6 days post-gavage, tapeworms were flushed
359 out of the small intestine, and washed in 1X Hanks Balanced Salt Solution (HBSS; Corning) (140
360 mg/L $CaCl_2$, 100 mg/L $MgCl_2.6H_2O$, 100 mg/L $MgSO_4.7H_2O$, 400 mg/L KCl, 60 mg/L KH_2PO_4,
361 350 mg/L $NaHCO_3$, 8 g/L NaCl, 48 mg/L Na_2HPO_4, 1 g/L D-glucose, no phenol red). Rodent care
362 was in accordance with protocols approved by the Institutional Animal Care and Use Committee
363 (IACUC) of the University of Wisconsin-Madison (M005573).

364 *In vitro* parasite culture

365 Biphasic parasite cultures were prepared based on the Schiller method[18]. Briefly, the solid
366 phase was made in 50 mL Erlenmeyer flasks by mixing 30% heat-inactivated defibrinated sheep
367 blood (Hemostat) with 70% agar base for 10 mL blood-agar mixture per flask. Fresh blood was
368 heat-inactivated at 56°C for 30 min then kept at 4°C and used repeatedly for one week by first
369 warming the blood to 37°C. The agar base was prepared from 8 g Difco nutrient agar and 1.75 g
370 NaCl in 350 mL water, autoclaved, and stored at 4°C. Before use, the agar base was microwaved
371 to liquify, and cooled to below 56°C before mixing with warmed blood. After the blood-agar
372 mixture solidified, 10 mL of Working Hanks 4 (WH4; 1X HBSS/4 g/L total glucose/1X antibiotic-
373 antimycotic (Sigma)) was added. Each flask was topped with a gas-permeable stopper (Jaece
374 Identi-plug) and pre-incubated at 37°C in hypoxia (3% CO_2/5% O_2/92% N_2) overnight before use.
375 Before tapeworms were transferred into the flasks, the liquid phase was adjusted to pH7.5 with
376 200 μL 7.5% $NaHCO_3$ (Corning). Tapeworms were first washed in WH4 for 10 mins at 37°C in

377 petri dishes pre-coated with 0.5% BSA to inhibit sticking. Transfers to pre-cultured flasks were
378 performed by gently lifting the worms with a stainless-steel hook (Moody Tools) and immersing
379 them in the liquid phase. Tapeworms were grown in hypoxia and transferred to fresh cultures every
380 3-4 days.

381 Fixation and DAPI Staining

382 Tapeworms were heat-killed by swirling in 75°C water for a few seconds until the worms
383 relaxed and elongated, then fixative (4% formaldehyde in Phosphate Buffered Saline with 0.3%
384 TritonX-100 (PBSTx)) was added immediately for 30 min-2hr at room temperature or overnight
385 at 4°C. For DAPI staining, samples were incubated in 1 μg/mL DAPI (Sigma) in PBSTx overnight
386 at 4°C and cleared in 80% glycerol/10 mM Tris pH7.5/1 mM EDTA overnight at room temperature
387 before mounting.

388 F-*ara*-EdU[31] uptake and staining

389 For F-*ara*-EdU pulse, tapeworms were incubated in 0.1 μM F-*ara*-EdU (Sigma) in 1%
390 DMSO at 37°C in WH4. Tapeworms were heat-killed (above) and fixed in 4% formaldehyde/10%
391 DMSO/1% NP40/PBSTx. Large tissues/worms were permeabilized by incubating in PBSTx at
392 room temp for several days. Additional permeabilization was achieved by treatment with 10
393 μg/mL Proteinase-K/0.1% SDS/PBSTx for 10-30 min at room temperature, fixed in 4%
394 formaldehyde/PBSTx for 10 min before samples were cut into small pieces or retained whole in
395 PBSTx. Samples were further permeabilized in PBSTx/10% DMSO/1% NP40 for 20min-1 hr
396 (depending on size) before performing the click-it reaction[44] with Oregon Green 488 Tyramide
397 (Invitrogen). Signal was detected using anti-Oregon Green 488-HRP antibody (1:1000;
398 Invitrogen) in K-block (5% Horse serum/0.45% fish gelatin/0.3% Triton-X/0.05% Tween-
399 20/PBS) [45] followed by Tyramide Signal Amplification (TSA) reaction [46]. Tiled confocal z-stacks

400 through the anterior of the worms were taken and cell numbers were counted using background
401 subtraction on Imaris software. F-*ara*-EdU^{+} cells were normalized to worm area from maximum
402 projections of the DAPI stain.

403 Irradiation

404 Most irradiation was performed using a CellRad irradiator (Faxitron Bioptics) at 200 Gy
405 (150 kV, 5 mA). Due to instrument failure, a cesium irradiator was used for one rescue experiment
406 with donors +/- HU (Fig. 6b) at 400 Gy (92±5 % cycling cell loss 3 days post-irradiation). In both
407 cases, lethal irradiation was determined as the dosage at which tapeworms degenerated and were
408 inviable after 30 days in culture. Irradiation was performed in WH4 in BSA-coated petri dishes.

409 Transcriptome assembly

410 RNA was collected from five regions: 1) head and neck, 2) immature proglottids, 3) mature
411 reproductive proglottids, 4) gravid proglottids, and 5) mixed larval stages isolated from beetles.
412 The first three regions covered the entirety of 3.5-week old adult tapeworms. Gravid proglottids
413 were taken from posteriors of 10-week old tapeworms. Paired-end libraries were constructed with
414 2 x 150 bp reads from a HiSeq2500 chip. 2 x ~30 million reads were obtained for each sample.
415 The transcriptome was assembled from three components: 1) map-based assembly, 2) *de novo*
416 assembly, and 3) Maker predictions from Wormbase Parasite. The map-based assembly was
417 performed using TopHat2 with the 2014 *H. diminuta* draft genome courtesy of Matt Berriman
418 (Wellcome Sanger Institute, UK). 15,859 transcripts were assembled using TopHat. *De novo*
419 assembly was performed using Velvet/Oases and resulted in 144,682 transcripts. There were
420 11,275 predicted Maker transcripts and 73.2% matched (>95% along the length) to the TopHat
421 transcripts. The remaining predicted transcripts that were not represented in the TopHat dataset
422 were added for a combined TopHat/predicted set of 17,651 transcripts. Most of the Oases

423 transcripts matched to the TopHat/predicted set but 35,300 or 24.4% of the Oases transcripts did
424 not (>75% match cut-off). These transcripts could be transcripts missed in the genome,
425 transcription noise, non-coding transcripts, or contamination. We found significant contamination
426 from beetle tissue in the larval tapeworm sample (more below). Initial filtering for contamination
427 excluded 1,388 transcripts (from beetle, rat, bacterial, and viral sources). At this point 51,563
428 transcripts were retained from the three methodologies described above and were processed for
429 further filtering.

430 There was significant contamination from beetle tissues that had adhered to the tapeworm
431 larvae, which produced transcripts with best hits to beetle proteins (*Ixodes scapularis,*
432 *Harpegnathos saltator, Monodelphis domestica, Nasonia vitripennis, Pediculus humanus*
433 *corporis, Solenopsis invicta, Tenebrio molitor,* or *Tribolium castaneum*). Most of the transcripts
434 were from the Oases *de novo* assembly and did not match the *H. diminuta* genome. Furthermore,
435 they were strongly over-represented in the larval sample only. To filter out beetle contamination,
436 we removed 11,918 transcripts from the Oases assembly without matches to the *H. diminuta*
437 genome that showed >90% expression (by RPKM) in the larval sample.

438 To the remaining 39,645 transcripts, we applied additional filters: 1) Remove transcripts if
439 average RPKM<1 unless the transcript is long (>1000 bp), has a long ORF (>500 bp) or is
440 annotated. 11,615 transcripts were removed as they met none of these criteria. 2) A stringent
441 expression cut-off was applied to the remaining Oases transcripts; transcripts were discarded if
442 average RPKM<5 and maximum RPKM<10 unless the transcripts were long (>1000 bp), had long
443 ORFs (>500 bp) or were annotated. 8,027 transcripts were removed. 3) 51 transcripts were
444 removed because they are mitochondrial or rRNAs. 4) An ORF size filter was applied to remove
445 all transcripts with ORF <300 bp unless they are annotated. 5,331 transcripts were removed. 5)

446 For the Maker predicted transcripts, expression and size filters were applied to remove transcripts
447 with expression <1 RPKM and size <500 bp. 275 transcripts were removed.
448 Our final transcriptome is comprised of 14,346 transcripts (84.9% TopHat, 8.4% Maker
449 predictions, 6.1% Oases with match to genome, and 0.6% Oases without match to genome). The
450 total transcriptome size is 34 Mb with average transcript length of 2,354 bp.

451 RNA-seq for differential gene expression analyses

452 Tissue was collected and immediately frozen on dry ice in 100 μL Trizol (Life
453 Technologies) before RNA extraction. Tissue homogenization was performed as the mixture was
454 in a semi-frozen state using RNase-free pestles and a pestle motor. RNA was purified using the
455 Direct-zol RNA MiniPrep kit (Zymo). RNA quality was assessed using Bioanalyzer, libraries were
456 prepared with TruSeq Stranded mRNAseq Sample Prep kit (Illumina), and sequenced on two lanes
457 on a HiSeq2500 chip. We performed paired-end sequencing and obtained ~20 million reads per
458 sample. Samples were obtained in triplicate. To identify irradiation-sensitive genes, 2 mm anterior
459 tapeworm fragments were cut from 10 worms after 3 days *in vitro*. To identify differentially
460 expressed transcripts across the neck A-P axis, 1 mm fragments were cut from 20 freshly obtained
461 6-day old tapeworms. Differential gene expression analysis was performed using CLC Genomics
462 Workbench (Qiagen) by mapping to our assembled transcriptome (above).

463 Cloning

464 Target genes were amplified using PCR with Platinum Taq (Life Technologies) from
465 cDNA generated from RNAs extracted from tapeworm anteriors to enrich for neck transcripts.
466 PCR products were inserted via TA-mediated cloning into the previously described vector
467 pJC53.2[47] pre-digested with *Eam11051*. Anti-sense riboprobes could be generated by *in vitro*

468 transcription with SP6 or T3 RNA polymerases. For RNAi, dsRNA was generated using T7 RNA
469 polymerase. For sequences and primers, refer to Supplemental Table 4.

470 *In situ* hybridization

471 WISH and FISH protocols were modified from previously published methods for
472 planarians[46] and the mouse bile-duct tapeworm *Hymenolepis microstoma* [48]. Tapeworms were heat
473 killed and fixed in 4% formaldehyde/10% DMSO/1% NP40/PBSTx for 30 min at room
474 temperature before washing and dehydration into methanol. Dehydrated samples were frozen at -
475 30°C for at least 2 days. After rehydration, samples were permeabilized in 10 μg/mL Proteinase-
476 K/0.1% SDS/PBSTx for 30 min, washed into 0.1 M Triethanolamine pH7-8 (TEA), 2.5 μL/mL
477 acetic anhydride was added for 5 min with vigorous swirling, acetic anhydride step was repeated,
478 washed in PBSTx, and post-fixed in 4% formaldehyde/PBSTx for 10 min. Probe synthesis,
479 hybridization, and staining were performed as previously described[46] using probe concentrations
480 at ~50 ng/mL for 16-48 hrs at 56°C. All probes were synthesized with either DIG or DNP haptens
481 and detected using the following antibodies, all at 1:2000: anti-DIG-AP (Sigma), anti-DIG-POD
482 (Roche), anti-DNP-HRP (Vector Labs). Colorimetric development was done using NBT
483 (Roche)/BCIP (Sigma) or with Fast-Blue (Sigma)[49]. Fluorescent signal was visualized after TSA
484 reaction[46]. DAPI staining and mounting were performed as described above.

485 Imaging

486 Confocal imaging was performed on a Zeiss LSM 880 with the following objectives:
487 20X/0.8 NA Plan-APOCHROMAT, 40X/1.3 NA Plan-APOCHROMAT, and 63X/1.4 NA Plan-
488 APOCHROMAT. WISH samples and whole-mount DAPI-stained worms were imaged using
489 Zeiss AxioZoom V16 macroscope. Image processing was performed using ImageJ for general
490 brightness/contrast adjustments, maximum-intensity projections, and tile stitching[50].

491 RNAi

492 dsRNA was synthesized as previously described[51] and resuspended at concentrations ~ 1.5-
493 2 μg/μL. For control injections, 1.5 kb dsRNA derived from *ccdB* and *camR*-containing insert of
494 the pJC53.2 vector was used[47]. 6-day old tapeworms were obtained and microinjected with dsRNA
495 using femtotips II via the Femtojet injection system (Eppendorf) to obtain spreading across the
496 first ~ 3-4 mm anterior of the tapeworm. The spread of injected fluids could be detected by a
497 temporary increase in opacity. 500 hPa injection pressure for 0.3-1 s was used per injection site.
498 Whole tapeworms were cultured *in vitro* for 3 days, 2 mm anterior fragments were amputated,
499 worms were re-injected with dsRNA on day 6, and cultured *in vitro* for an additional 9 days before
500 termination.

501 qPCR for target gene knockdown efficacy

502 Whole worms (6-days old) were injected with dsRNA throughout and frozen in Trizol on
503 dry ice after 6 days *in vitro* for RNA extraction according to manufacturer's protocol and DNAse
504 (Promega) treatment for 30 min at 37°C. cDNA synthesis was performed using SuperScriptIII
505 First-Strand Synthesis System (Invitrogen) with Oligo$(dT)_{20}$ primers followed by iScript cDNA
506 Synthesis Kit (Bio-Rad). qPCR was performed using GoTaq Mastermix (Promega) on a
507 StepOnePlus real-time PCR machine (Applied Biosystems). *60S ribosomal protein L13*
508 (*60Srpl13)* was used as an internal normalization control. For primers refer to Supplemental Table
509 4.

510 Hydroxyurea (HU) treatment

511 Tapeworms were treated with HU (Sigma) or HBSS (for controls) every day for a total of
512 6 days. HU stock solution was made fresh every day at 2 M in HBSS. 250 μL was added to each
513 flask of tapeworms for final concentration of 50 mM. HU is unstable at 37°C so worms were

514 transferred into fresh HU-containing media every two days, and fresh HU was added every other
515 day.

516 Cell transplantations

517 For dissociated cell preparations, tapeworms were placed in a drop of calcium-magnesium
518 free HBSS (CMF HBSS, Gibco), minced into small pieces with a tungsten needle, incubated in
519 3X Trypsin-EDTA (Sigma) in CMF HBSS for 30 min at 37°C and dissociated using a dounce
520 homogenizer (Kontes). Cells were pelleted by centrifugation at 250 g for 5 min. The cell pellet
521 was washed in CMF HBSS and passed through cell strainers at 100 μm, 40 μm, 20 μm, and 10
522 μm (Falcon and Sysmex) with one spin and wash in between. Cells were pelleted and resuspended
523 in 200-400 μL WH4 with 0.05% BSA. Cell injections were performed using the Cell Tram Oil 4
524 injection system (Eppendorf) into the necks of irradiated worms. For +/- HU donors, cell
525 concentrations were measured using a hemocytometer and normalized (to ~10^8 cells/mL) to ensure
526 equal numbers of cells were injected. After 3 days *in vitro,* 5 mm anterior fragments were
527 amputated and grown for an additional 27 days.

528 Statistical Analysis.

529 Statistical analyses were performed using Prism7 software (GraphPad Prism). All
530 experiments were repeated at least twice. All measurements were taken from distinct samples.
531 Error bars, statistical tests, number of replicates (N) and sample sizes (n) are indicated in
532 corresponding figure legends. Either Dunnett's or Tukey's multiple comparison tests were used
533 for one-way ANOVAs based on Prism recommendation. SD=standard deviation. P-values: ns=
534 not significant, *= $p \leq 0.5$, ****= $p \leq 0.0001$.

535

536 **References**

537 1. Del Brutto, O. H. Human cysticercosis (*Taenia solium*). *Trop Parasitol* **3,** 100–103
538 (2013).
539 2. Craig, P. & Ito, A. Intestinal cestodes. *Curr. Opin. Infect. Dis.* **20,** 524–532 (2007).
540 3. Roberts, L. S. Development of *Hymenolepis diminuta* in its definitive host in *Biology of*
541 *the Tapeworm Hymenolepis diminuta* 357–423 (Academic Press Inc., NY, 1980).
542 4. Arai, H. P. (Ed.) *Biology of the Tapeworm Hymenolepis diminuta*. (Academic Press, Inc.,
543 1980).
544 5. Read, C. P. Longevity of the tapeworm, *Hymenolepis diminuta*. *J. Parasitol.* **53,** 1055–
545 1056 (1967).
546 6. Newmark, P. A. & Sánchez Alvarado, A. Not Your Father's Planarian: A Classic Model
547 Enters The Era Of Functional Genomics. *Nat. Rev. Genet.* **3,** 210–219 (2002).
548 7. Reddien, P. W. The Cellular and Molecular Basis for Planarian Regeneration. *Cell* **175,**
549 327–345 (2018).
550 8. Baguñà, J. The planarian neoblast: the rambling history of its origin and some current
551 black boxes. *Int. J. Dev. Biol.* **56,** 19–37 (2012).
552 9. Collins, J., III *et al.* Adult somatic stem cells in the human parasite *Schistosoma mansoni*.
553 *Nature* **494,** 476–479 (2013).
554 10. Koziol, U., Rauschendorfer, T., Zanon Rodríguez, L., Krohne, G. & Brehm, K. The
555 unique stem cell system of the immortal larva of the human parasite *Echinococcus*
556 *multilocularis*. *EvoDevo* **5,** 10 (2014).
557 11. Koziol, U. *et al.* A Novel Terminal-Repeat Retrotransposon in Miniature (TRIM) Is
558 Massively Expressed in *Echinococcus multilocularis* Stem Cells. *Genome Biol Evol* **7,**
559 2136–2153 (2015).
560 12. Wang, B., Collins, J., III & Newmark, P. A. Functional genomic characterization of
561 neoblast-like stem cells in larval *Schistosoma mansoni*. *Elife* **2,** e00768 (2013).
562 13. Koziol, U., Domínguez, M. F., Marín, M., Kun, A. & Castillo, E. Stem cell proliferation
563 during in vitro development of the model cestode *Mesocestoides corti* from larva to adult
564 worm. *Front. Zool.* **7,** 22 (2010).
565 14. Collins, J., III. Platyhelminthes. *Current Biology* **27,** R252–R256 (2017).
566 15. Collins, J., III, Wendt, G. R., Iyer, H. & Newmark, P. A. Stem cell progeny contribute to
567 the schistosome host-parasite interface. *Elife* **5,** 243 (2016).
568 16. Brehm, K. & Koziol, U. On the importance of targeting parasite stem cells in anti-
569 echinococcosis drug development. *Parasite* **21,** 72 (2014).
570 17. Rozario, T. & Newmark, P. A. A confocal microscopy-based atlas of tissue architecture in
571 the tapeworm *Hymenolepis diminuta*. *Exp. Parasitol.* **158,** 31–41 (2015).
572 18. Schiller, E. L. A simplified method for the in vitro cultivation of the rat tapeworm,
573 *Hymenolepis diminuta*. *J. Parasitol.* **51,** 516–518 (1965).
574 19. Goodchild, C. G. Transfaunation and Repair of Damage in the Rat Tapeworm,
575 *Hymenolepis diminuta*. *J. Parasitol.* **44,** 345–351 (1958).
576 20. Bolla, R. I. & Roberts, L. S. Developmental physiology of cestodes. IX. Cytological
577 characteristics of the germinative region of *Hymenolepis diminuta*. *J. Parasitol.* **57,** 267–
578 277 (1971).

579 21. Sulgostowska, T. The development of organ systems in cestodes. I. A study of histology
580 of *Hymenolepis diminuta* (Rudolphi, 1819)(Hymenolepididae). *Acta Parasitologica*
581 *Polonica* **20,** 449–462 (1972).
582 22. Neef, A. B. & Luedtke, N. W. Dynamic metabolic labeling of DNA in vivo with
583 arabinosyl nucleosides. *Proceedings of the National Academy of Sciences* **108,** 20404–
584 20409 (2011).
585 23. Solana, J. *et al.* Defining the molecular profile of planarian pluripotent stem cells using a
586 combinatorial RNAseq, RNA interference and irradiation approach. *Genome Biol.* **13,** R19
587 (2012).
588 24. Eisenhoffer, G. T., Kang, H. & Sánchez Alvarado, A. Molecular Analysis of Stem Cells
589 and Their Descendants during Cell Turnover and Regeneration in the Planarian *Schmidtea*
590 *mediterranea*. *Cell Stem Cell* **3,** 327–339 (2008).
591 25. Koziol, U. & Castillo, E. Cell proliferation and differentiation in cestodes. *Research in*
592 *Helminths* 121–138 (2011).
593 26. Collins, J. N. R. & Collins, J., III. Tissue Degeneration following Loss of *Schistosoma*
594 *mansoni* cbp1 Is Associated with Increased Stem Cell Proliferation and Parasite Death In
595 Vivo. *PLoS Pathog* **12,** e1005963 (2016).
596 27. Cheever, A. W., Macedonia, J. G., Mosimann, J. E. & Cheever, E. A. Kinetics of Egg
597 Production and Egg Excretion by *Schistosoma mansoni* and *S. japonicum* in Mice Infected
598 with a Single Pair of Worms. *The American Journal of Tropical Medicine and Hygiene*
599 **50,** 281–295 (1994).
600 28. Lumsden, R. D. & Specian, R. The morphology, histology, and fine structure of the adult
601 stage of the cyclophyllidean tapeworm *Hymenolepis diminuta* in *Biology of the Tapeworm*
602 *Hymenolepis diminuta.* 157–280 (Academic Press Inc., NY, 1980).
603 29. Tsai, I. J. *et al.* The genomes of four tapeworm species reveal adaptations to parasitism.
604 *Nature* **496,** 57–63 (2013).
605 30. van Wolfswinkel, J. C., Wagner, D. E. & Reddien, P. W. Single-Cell Analysis Reveals
606 Functionally Distinct Classes within the Planarian Stem Cell Compartment. *Cell Stem Cell*
607 **15,** 326–339 (2014).
608 31. Fincher, C. T., Wurtzel, O., de Hoog, T., Kravarik, K. M. & Reddien, P. W. Cell type
609 transcriptome atlas for the planarian Schmidtea mediterranea. *Science* **360,** eaaq1736
610 (2018).
611 32. Zeng, A. *et al.* Prospectively Isolated Tetraspanin+ Neoblasts Are Adult Pluripotent Stem
612 Cells Underlying Planaria Regeneration. *Cell* **173,** 1593–1608.e20 (2018).
613 33. Hu, X. *et al.* Gene knockout of *Zmym3* in mice arrests spermatogenesis at meiotic
614 metaphase with defects in spindle assembly checkpoint. *Cell Death Dis* **8,** e2910 (2017).
615 34. Leung, J. W. C. *et al.* ZMYM3 regulates BRCA1 localization at damaged chromatin to
616 promote DNA repair. *Genes Dev.* **31,** 260–274 (2017).
617 35. Gdula, D. A., Gerasimova, T. I. & Corces, V. G. Genetic and molecular analysis of the
618 gypsy chromatin insulator of Drosophila. *Proc. Natl. Acad. Sci. U.S.A.* **93,** 9378–9383
619 (1996).
620 36. Pierson, L. *et al.* RNA interference in a cestode reveals specific silencing of selected
621 highly expressed gene transcripts. *Int. J. Parasitol.* **40,** 605–615 (2010).
622 37. Mizukami, C. *et al.* Gene silencing in *Echinococcus multilocularis* protoscoleces using
623 RNA interference. *Parasitol. Int.* **59,** 647–652 (2010).

624 38. Spiliotis, M. *et al. Echinococcus multilocularis* primary cells: improved isolation, small-
625 scale cultivation and RNA interference. *Mol. Biochem. Parasitol.* **174,** 83–87 (2010).
626 39. Plass, M. *et al.* Cell type atlas and lineage tree of a whole complex animal by single-cell
627 transcriptomics. *Science* **360,** eaaq1723 (2018).
628 40. Sikes, J. M. & Newmark, P. A. Restoration of anterior regeneration in a planarian with
629 limited regenerative ability. *Nature* **500,** 77–80 (2013).
630 41. Liu, S. Y. *et al.* Reactivating head regrowth in a regeneration-deficient planarian species.
631 *Nature* **500,** 81–84 (2013).
632 42. Umesono, Y. *et al.* The molecular logic for planarian regeneration along the anterior-
633 posterior axis. *Nature* **500,** 73–76 (2013).
634 43. Koziol, U., Jarero, F., Olson, P. D. & Brehm, K. Comparative analysis of Wnt expression
635 identifies a highly conserved developmental transition in flatworms. *BMC Biol.* **14,** 1
636 (2016).
637 44. Salic, A. & Mitchison, T. J. A chemical method for fast and sensitive detection of DNA
638 synthesis in vivo. *Proceedings of the National Academy of Sciences* **105,** 2415–2420
639 (2008).
640 45. Collins, J., III, King, R. S., Cogswell, A., Williams, D. L. & Newmark, P. A. An atlas for
641 *Schistosoma mansoni* organs and life-cycle stages using cell type-specific markers and
642 confocal microscopy. *PLoS Negl Trop Dis* **5,** e1009 (2011).
643 46. King, R. S. & Newmark, P. A. In situ hybridization protocol for enhanced detection of
644 gene expression in the planarian *Schmidtea mediterranea*. *BMC Dev. Biol.* **13,** 8 (2013).
645 47. Collins, J., III *et al.* Genome-wide analyses reveal a role for peptide hormones in planarian
646 germline development. *PLoS Biol.* **8,** e1000509 (2010).
647 48. Olson, P. D. *et al.* Genome-wide transcriptome profiling and spatial expression analyses
648 identify signals and switches of development in tapeworms. *EvoDevo* **9,** R991 (2018).
649 49. Currie, K. W. *et al.* HOX gene complement and expression in the planarian *Schmidtea*
650 *mediterranea*. *EvoDevo* **7,** 7 (2016).
651 50. Preibisch, S., Saalfeld, S. & Tomancak, P. Globally optimal stitching of tiled 3D
652 microscopic image acquisitions. *Bioinformatics* **25,** 1463–1465 (2009).
653 51. Rouhana, L. *et al.* RNA interference by feeding in vitro-synthesized double-stranded RNA
654 to planarians: methodology and dynamics. *Dev. Dyn.* **242,** 718–730 (2013).

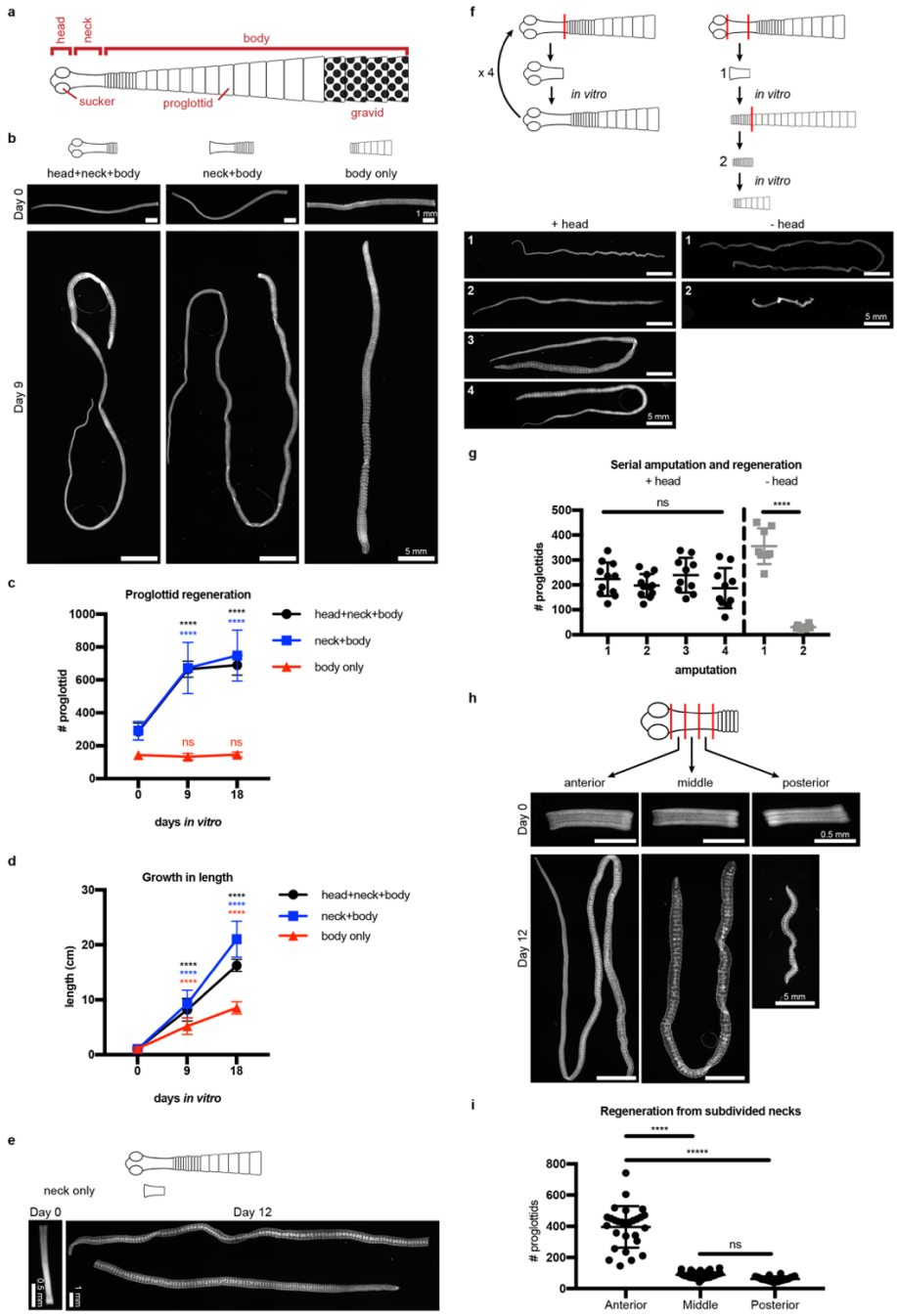

Figure 1. Regeneration competence of *H. diminuta*. a, Schematic of *H. diminuta* adults. **b**, DAPI-stained 1 cm fragments grown *in vitro*. **c-d**, Quantification of proglottid number and growth in length from (**b**). Error bars=SD, N=2-5, n=7-21; one-way ANOVA with Dunnett's multiple comparison test, compared to Day 0. **e**, Representative DAPI-stained "neck only" fragment regeneration. **f-g**, 2 mm anterior fragments, with or without the head, grown *in vitro* for 12-15 days and then re-amputated serially. Error bars=SD, +head: one-way ANOVA with Tukey's multiple comparison test, -head: Student's t-test. **h-i**, DAPI-stained 1 mm fragments from the anterior, middle, and posterior of the neck grown *in vitro*. Error bars=SD, N=3, n=22-29, one-way ANOVA with Tukey's multiple comparison test.

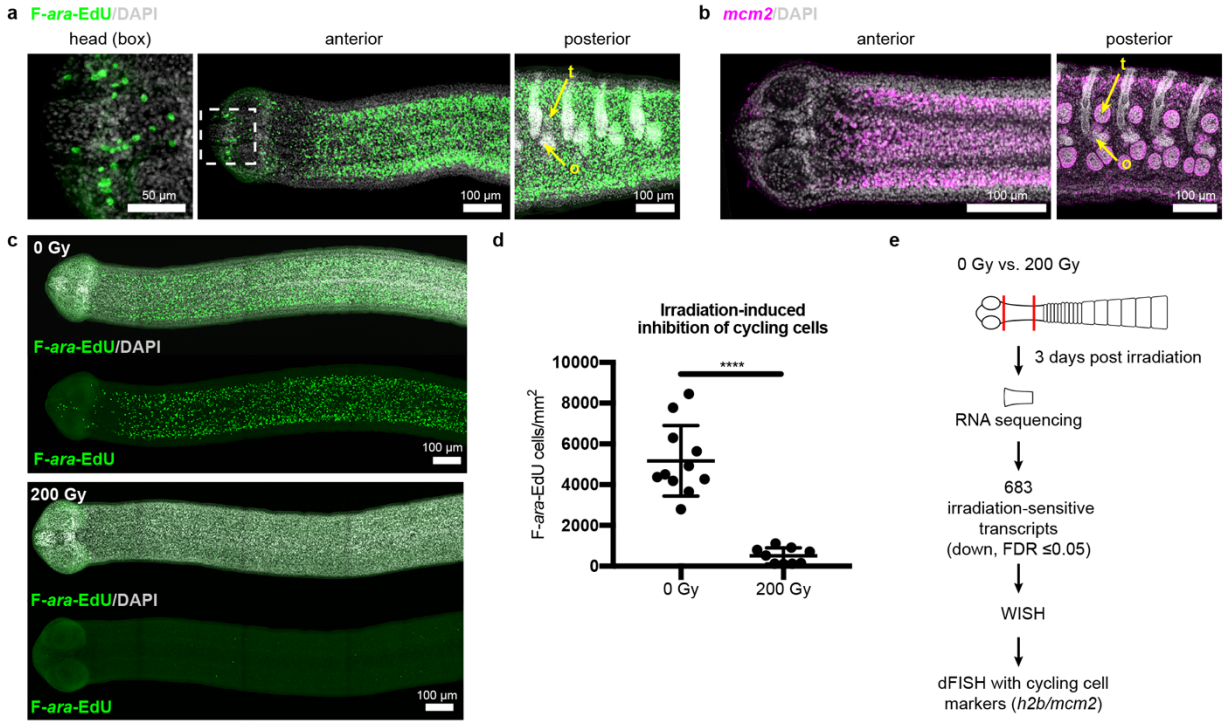

Figure 2. Cycling somatic cells are distributed throughout the tapeworm body and are irradiation sensitive. a-b, Maximum-intensity projections of confocal sections showing distribution of cycling cells by 2 hr uptake of F-*ara*-EdU (**a**) or FISH for *mcm2* (**b**). Fewer cycling cells were found in the head (box), while abundant cycling cells were observed in both somatic and gonadal tissues throughout the body. t=testis, o=ovary. **c**, Maximum-intensity projections of tile-stitched confocal sections after 1 hr uptake of F-*ara*-EdU (green) 3 days post-irradiation. **d**, Quantification of F-*ara*-EdU^{+} cell inhibition from (**c**). Error bars=SD, N=2, n=11 and 9, Student's t-test. **e**, RNA-seq strategy to identify genes expressed in cycling cells.

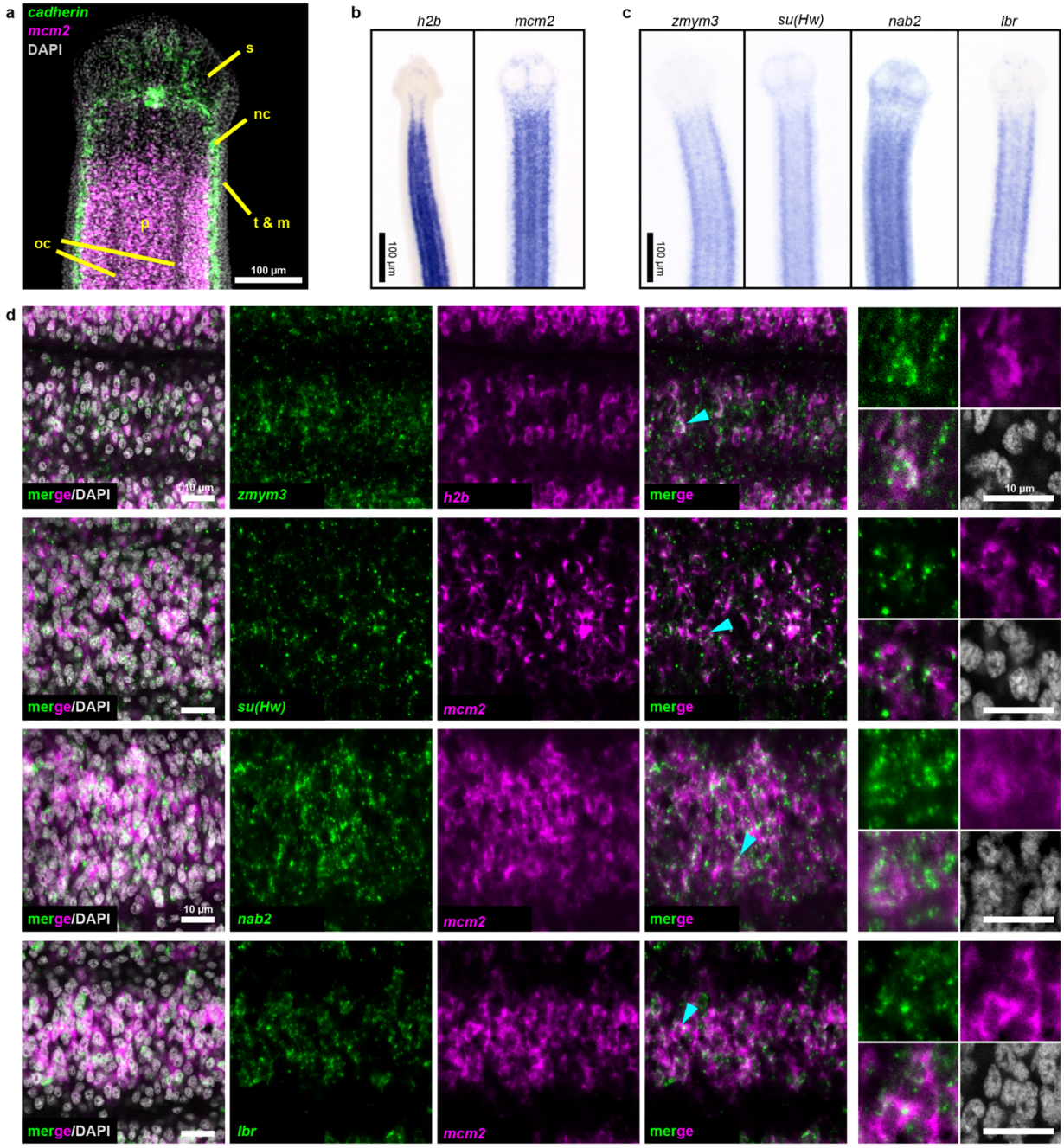

Figure 3. Expression screening for cycling cell markers. a, Confocal section of a tapeworm anterior. Cycling cells (*mcm2*: magenta) in the neck parenchyma between the nerve cords (*cadherin*: green). s: sucker, nc: nerve cord, oc: osmoregulatory canal, t: tegument, m: muscle, and p: parenchyma. **b**, WISH of known cycling-cell markers *h2b* and *mcm2*. **c**, WISH for irradiation-sensitive genes expressed in the neck parenchyma. **d**, Confocal sections of dFISH for irradiation-sensitive genes (green) with *h2b* or *mcm2* (magenta) from neck parenchyma. Cyan arrowheads indicate cells magnified at the far right.

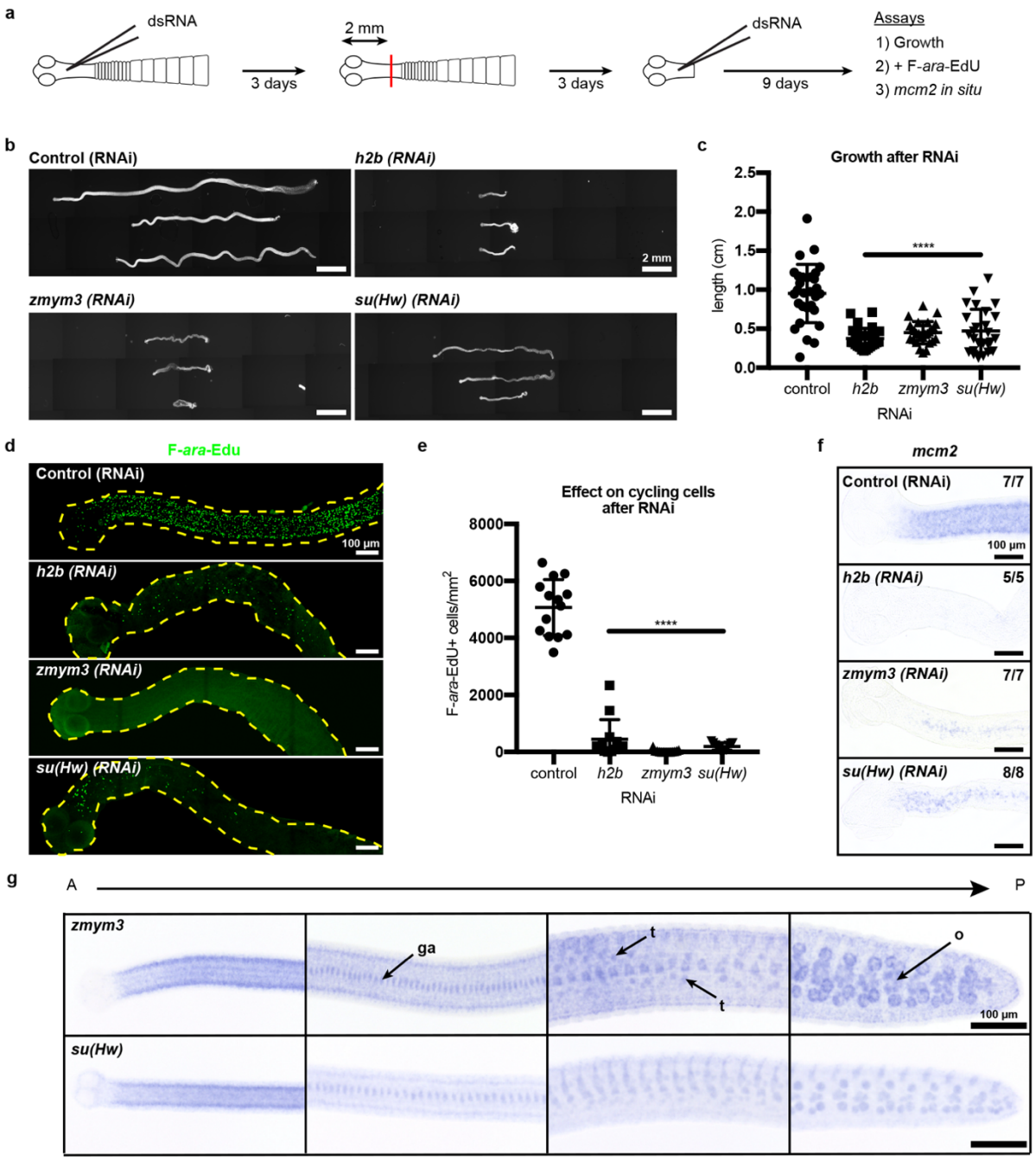

683

684 **Figure 4. RNAi to identify genes required for growth and regeneration in *H. diminuta*. a**,
685 Schematic of RNAi paradigm. **b**, DAPI-stained worms after RNAi knockdown of *h2b, zmym3*,
686 and *su(Hw)*. **c**, Quantification of worm lengths after RNAi. Error bars=SD, N=3-4, n=26-37, one-
687 way ANOVA with Dunnett's multiple comparison test compared to control. **d-e**, Maximum-
688 intensity projections (**d**) and quantification (**e**) of cycling-cell inhibition after 1 hr F-*ara*-EdU
689 uptake following RNAi. Worms with degenerated necks were excluded from analysis. Error
690 bars=SD, N=3, n=11-14, one-way ANOVA with Dunnett's multiple comparison test compared to
691 control. **f**, *mcm2* WISH on worm anteriors after RNAi. **g**, WISH of *zmym3* and *su(Hw)* sampled
692 from anterior to posterior of adult 6-day old worms. ga: genital anlagen; t: testis; o: ovary.

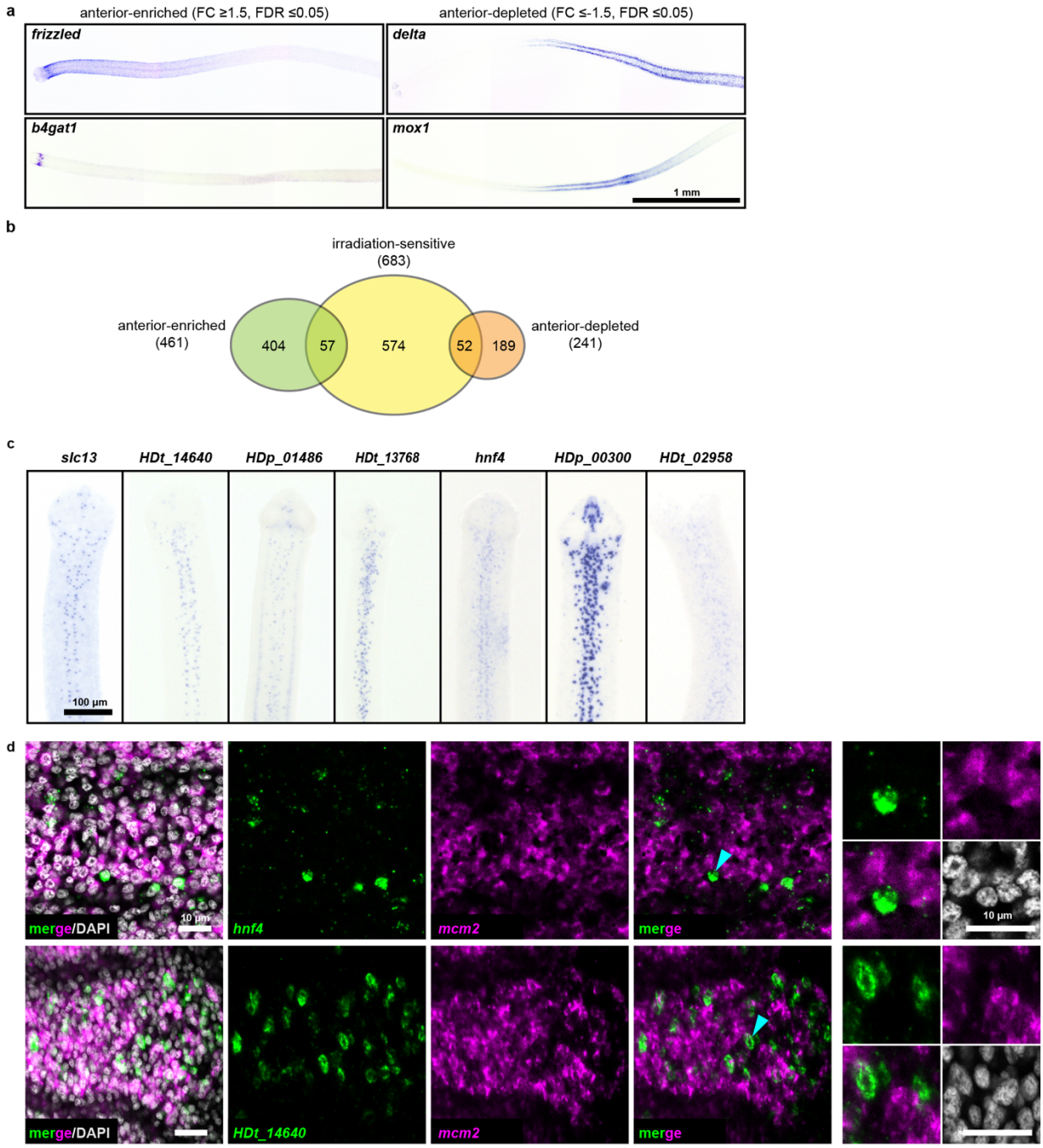

Figure 5. RNA-seq identifies anterior-enriched genes that are expressed predominantly in non-cycling cells. a, WISH of tapeworm anteriors for genes that were anterior-enriched (FC ≥1.5, FDR ≤0.05) or -depleted (FC ≤-1.5, FDR ≤0.05) by RNA-seq. Panels oriented anterior facing left. **b,** Differential gene expression analyses of 1 mm anterior, middle, and posterior neck fragments overlaid with irradiation-sensitive transcripts. **c**, WISH of genes that were anterior-enriched and irradiation-sensitive by RNA-seq that showed expression in a subset of cells in the neck parenchyma. **d**, Confocal sections from dFISH of anterior-enriched genes (green) and *mcm2* (magenta). Cyan arrowheads indicate cells that are magnified at the far right.

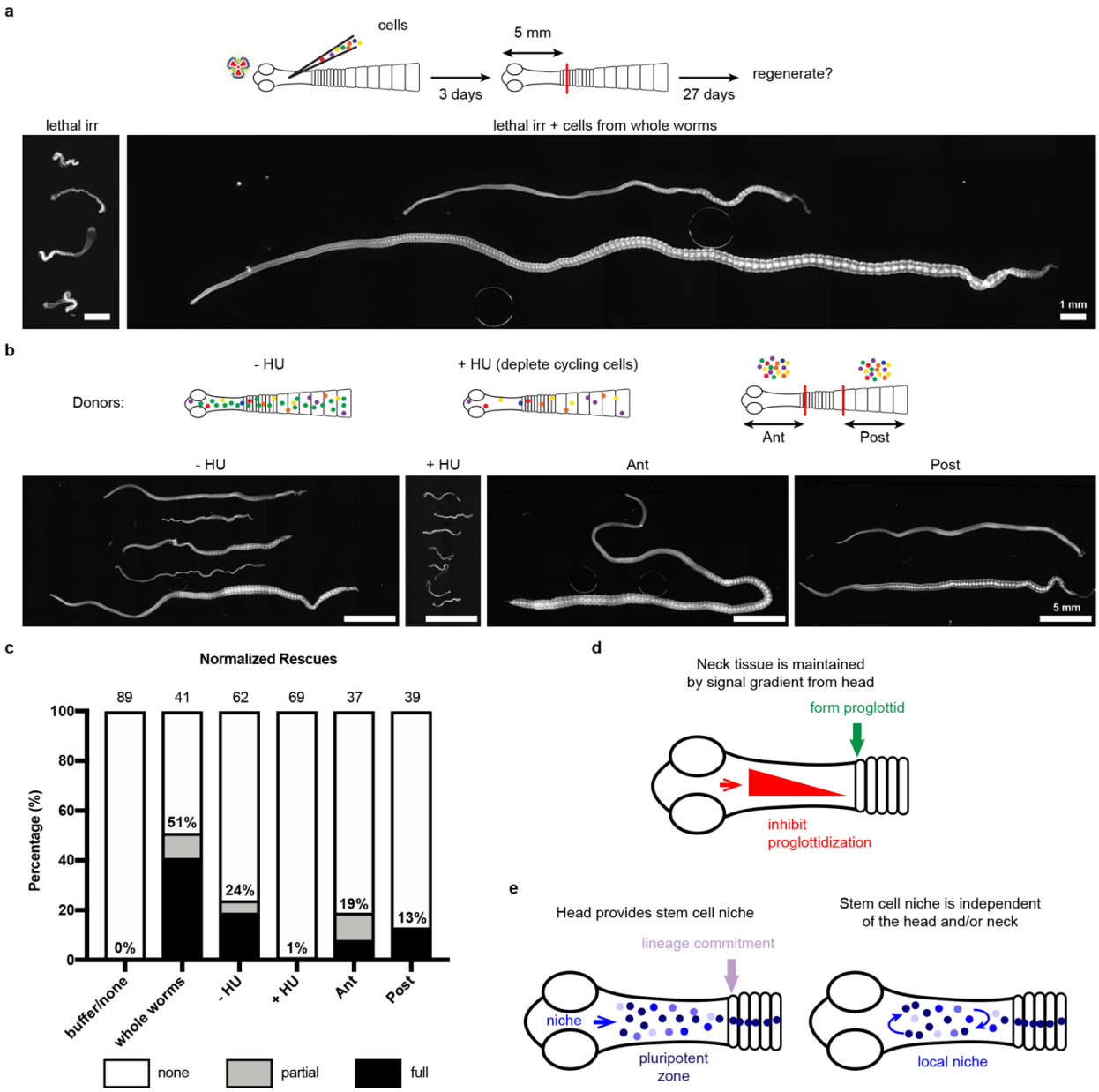

Figure 6. Stem cell activity depends on cycling cells but is not confined to cells from the neck. **a-b**, DAPI-stained worms after rescue with cell transplantations from whole-worm donors (**a**) or sourced from depicted donors (**b**). **c**, Quantification of rescue phenotypes from pooled experiments. Number of animals listed above bars. **d**, Model for head-dependent neck maintenance and proglottid formation. **e**, Models of head-dependent or -independent stem cell niches.

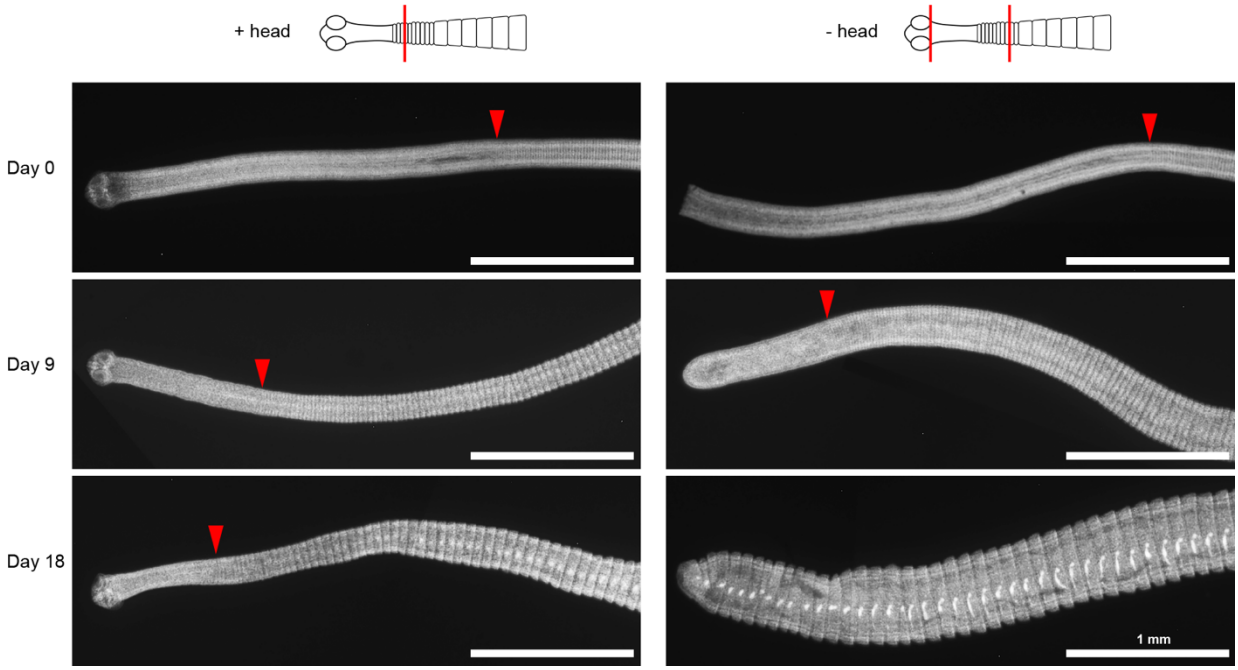

Figure 1–figure supplement 1. Unsegmented neck is depleted after decapitation. DAPI-stained worms with or without decapitation were cultured *in vitro* for the indicated number of days. Red arrowheads mark the position of the first visible proglottid. After 18 days *in vitro,* the neck tissue is no longer identifiable in -head worms.

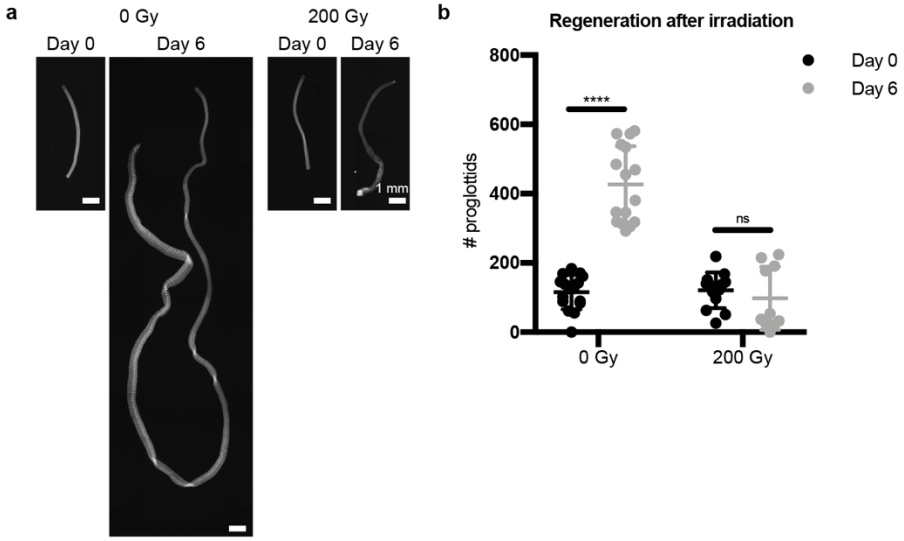

713
714 **Figure 2–figure supplement 1. Irradiation inhibits tapeworm regeneration. a**, DAPI staining
715 of 5 mm anterior fragments from control and irradiated worms before and after 6 days *in vitro*
716 culture. **b**, Quantification of **(a)**. Error bars=SD, N=2, n= 10-16, one-way ANOVA with Tukey's
717 multiple comparison test.
718

719

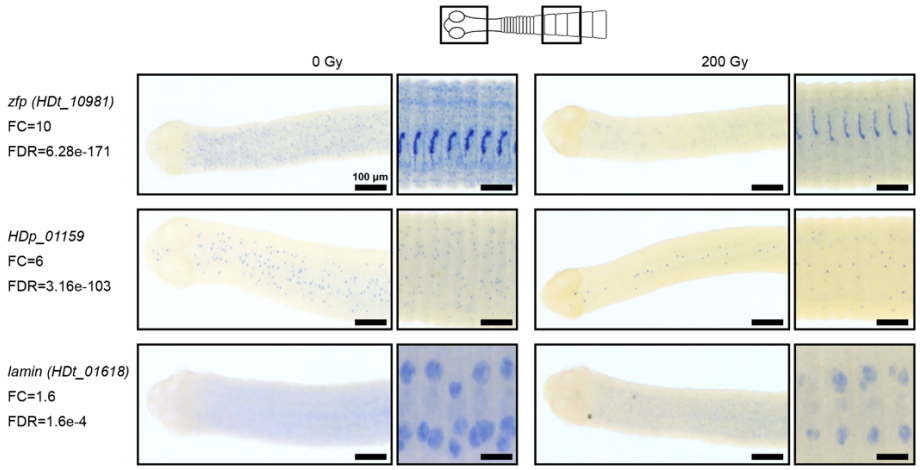

720

721 **Figure 2–figure supplement 2. Validation of RNA-seq by WISH after irradiation.** WISH (with
722 Fast-Blue Development) from two regions of the tapeworm: anterior (left) and body (right), 3 days
723 post-irradiation.

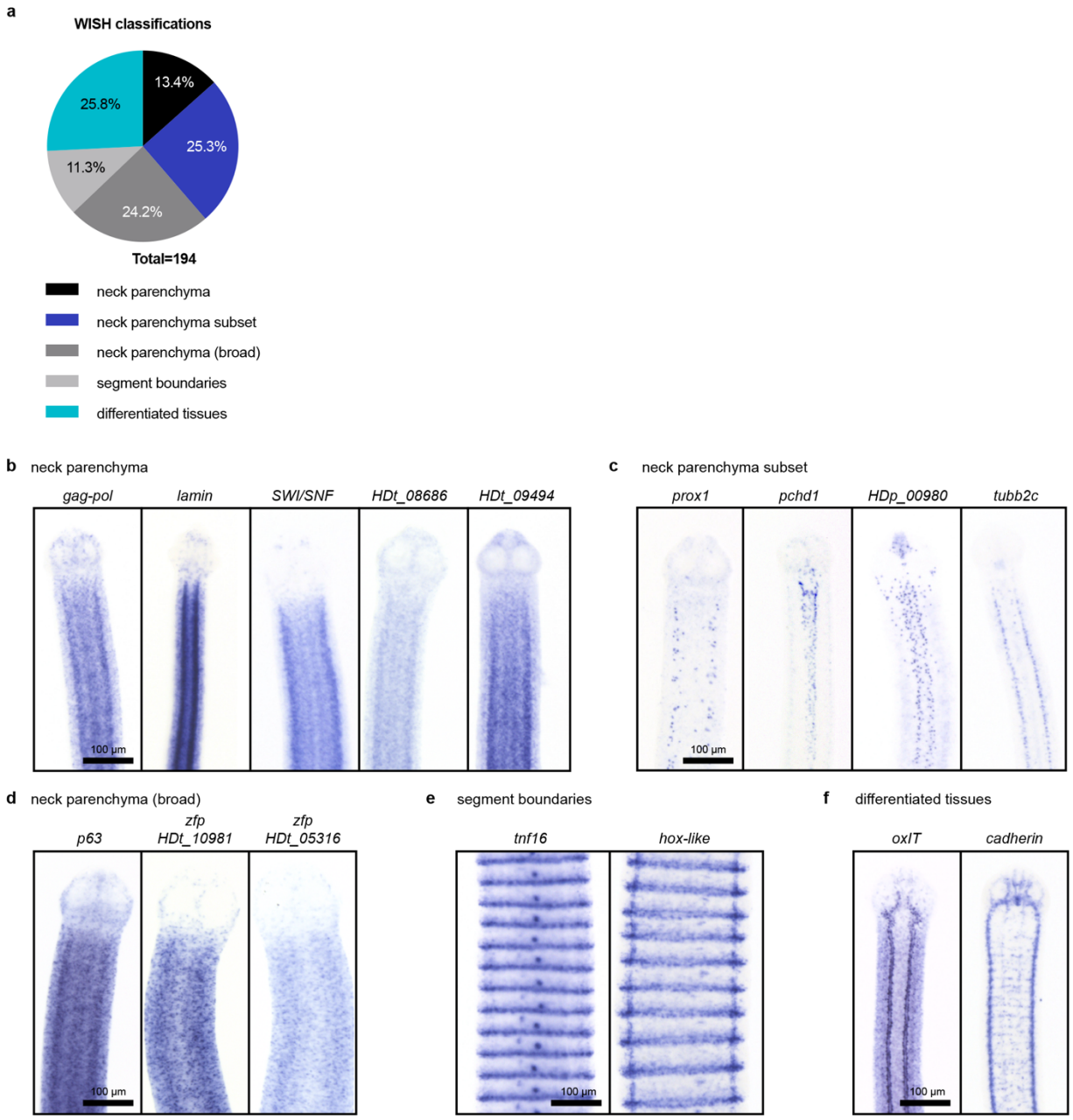

Figure 3–figure supplement 1. WISH patterns of irradiation-sensitive genes identified using RNA-seq. a, Classification of WISH expression patterns of irradiation-sensitive genes. **b-f**, Examples of genes expressed in the neck parenchyma (**b**), in subsets of cells within the neck (**c**), in neck parenchyma and broadly toward the animal edge where differentiated muscle and tegument are located (**d**), at segment boundaries (**e**), and in differentiated tissues (**f**) like the osmoregulatory canals (left) and nervous system (right).

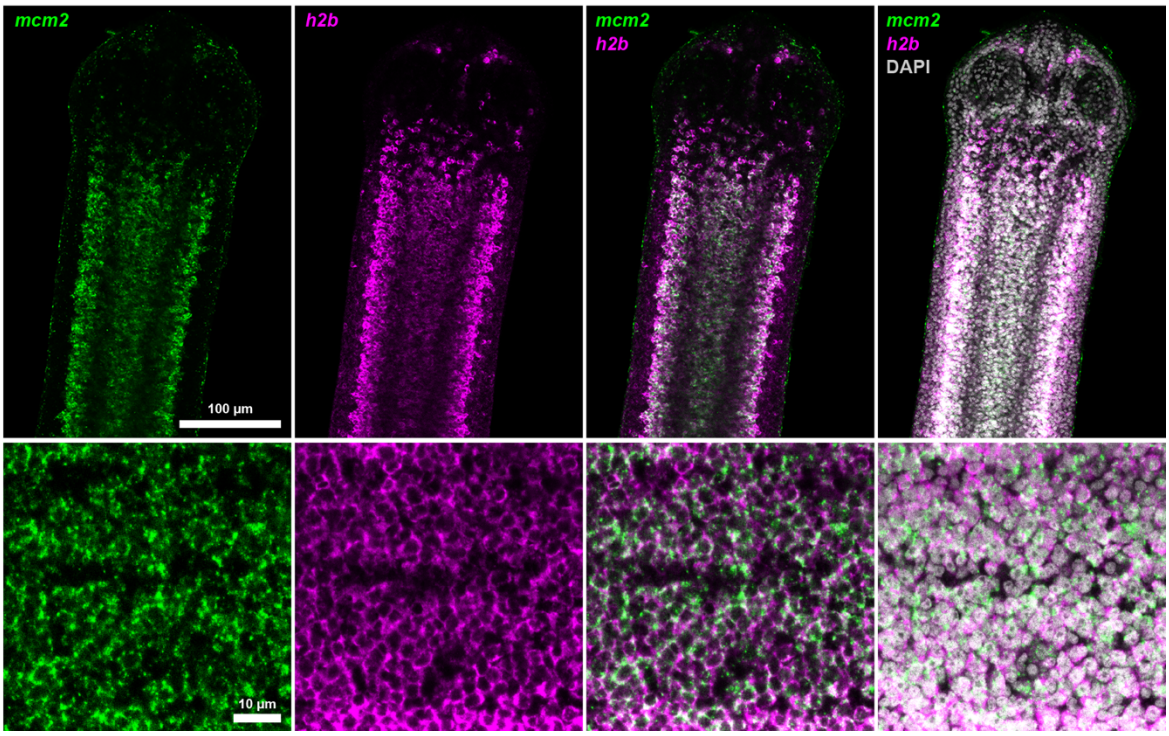

Figure 3–figure supplement 2. Colocalization of *mcm2* and *h2b*. Confocal section of dFISH to detect *mcm2* (green) and *h2b* (magenta) in the neck parenchyma at low(top) and high (bottom) magnification.

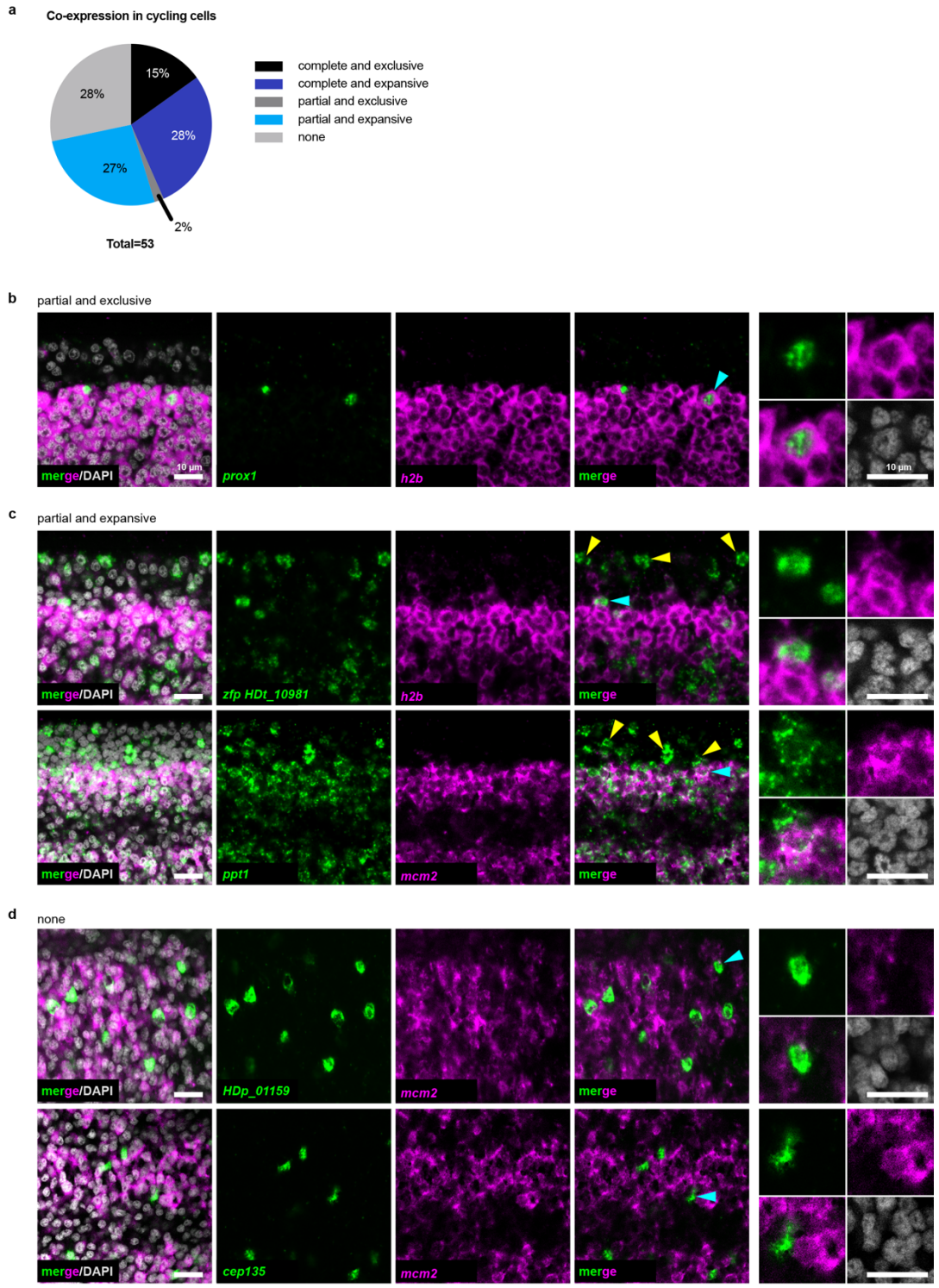

Figure 3–figure supplement 3. The cycling somatic cell population is heterogeneous. a, Summary of different co-expression patterns obtained from 53 dFISH experiments. Also refer to Supplemental Table 2. **b-d**, Confocal sections of dFISH to detect irradiation-sensitive genes (green) with *h2b* or *mcm2* (magenta). Cyan arrowheads indicate cells magnified at the far right. For (**c**), yellow arrowheads point to examples of expression in non-cycling cells.

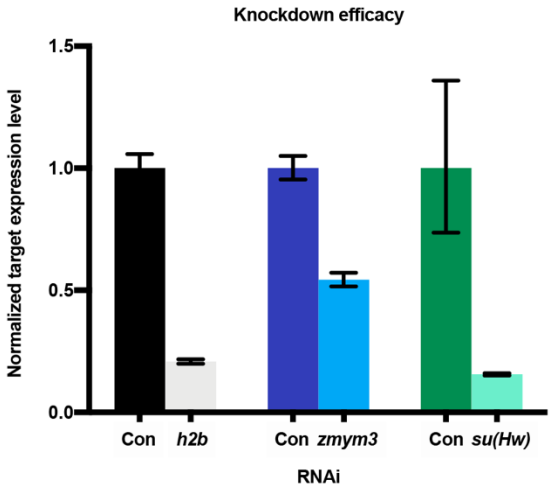

742
743 **Figure 4–figure supplement 1. Validation of target gene knockdown by quantitative PCR.**
744 Knockdown of *h2b*, *zmym3*, or *su(Hw)* in whole worms observed after RNAi. Error bars: RQ
745 min/max, N=2, n=3 each

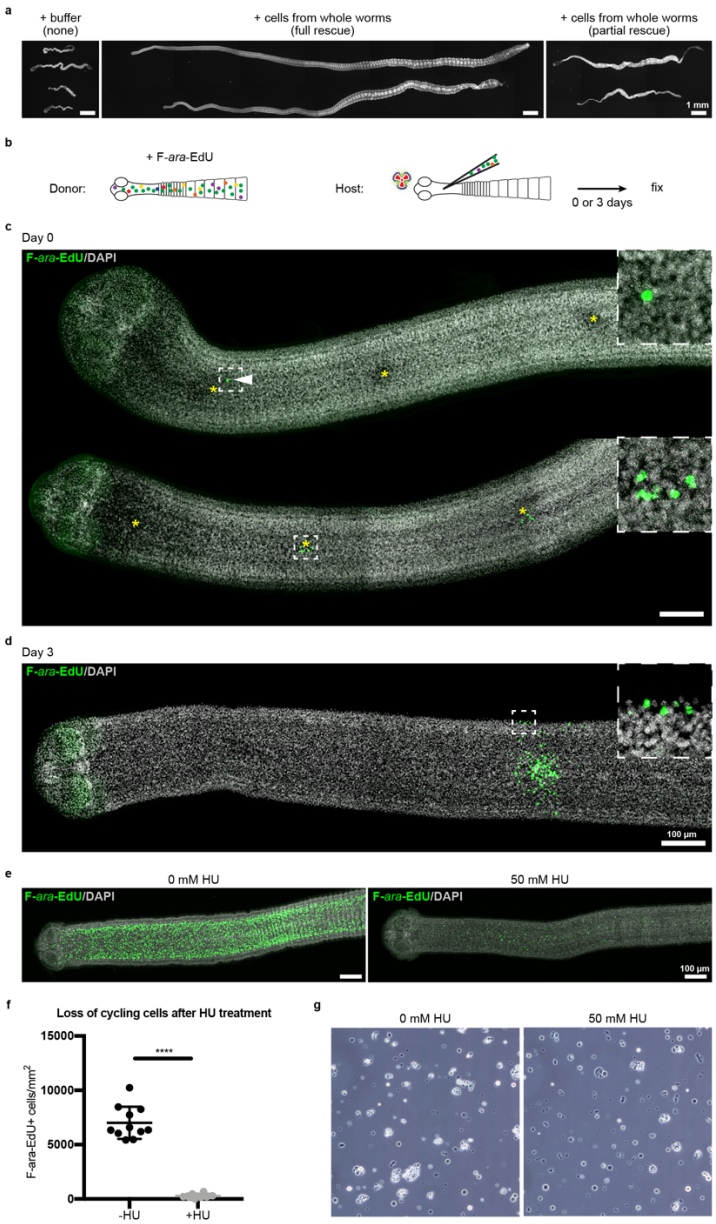

Figure 6–figure supplement 1. Stem cell activity depends on cycling cells. a, DAPI-stained worms showing phenotypes observed after attempted rescue of irradiation-induced lethality. No rescue results in degenerated worms with no proglottids, full rescue results in normal worms with multiple proglottids, and partial rescue refers to worms with visible proglottids but with defects such as contracted necks. **b**, Schematic for rescue experiment using donors with labeled cycling cells. **c-d**, Maximum-intensity projections of tile-stitched confocal sections 0 or 3 days post-transplanation according to (**b**). Injections sites marked with asterisks. White arrowhead points to a single transplanted cell. After 3 days, large colonies of F-*ara*-EdU^{+} (green) cells could be detected with some labeled cells incorporated into terminally differentiated tissues at the animal edge (inset). **e**, Maximum-intensity projections of tile-stitched confocal sections after 1 hr F-*ara*-EdU uptake (green) from control worms or worms cultured with hydroxyurea (HU) for 6 days. **f**, Quantification of cycling cells from (**e**). Error bars=SD, N=3, n=11 and 8, Student's t-test. **g**, Cell morphology with or without HU treatment prior to transplantation.

760 **Supplemental Table 1. Irradiation-sensitive transcripts identified by RNA-seq.**

761

762 **Supplemental Table 2. Summary of dFISH experiments with irradiation-sensitive genes and**

763 **cycling cell markers *h2b* and/or *mcm2*.**

764

765 **Supplemental Table 3. Anterior-enriched and anterior-depleted neck transcripts by RNA-**

766 **seq.**

767

768 **Supplemental Table 4. Sequences and primers for all genes reported.**